Supplementary information

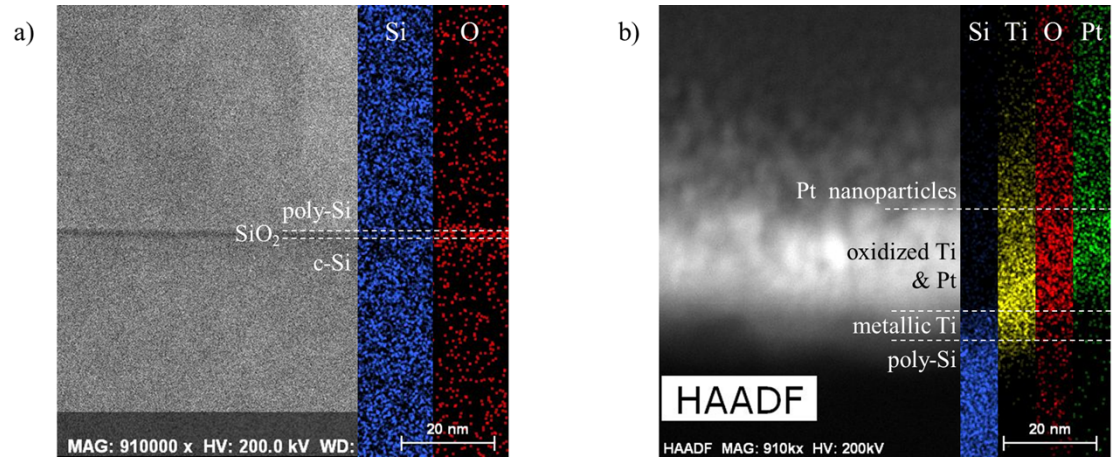

Figure S1 TEM and EDS images on a) SiO2 tunneling oxide passivation contact and b) Ti protection/Pt catalyst layers.

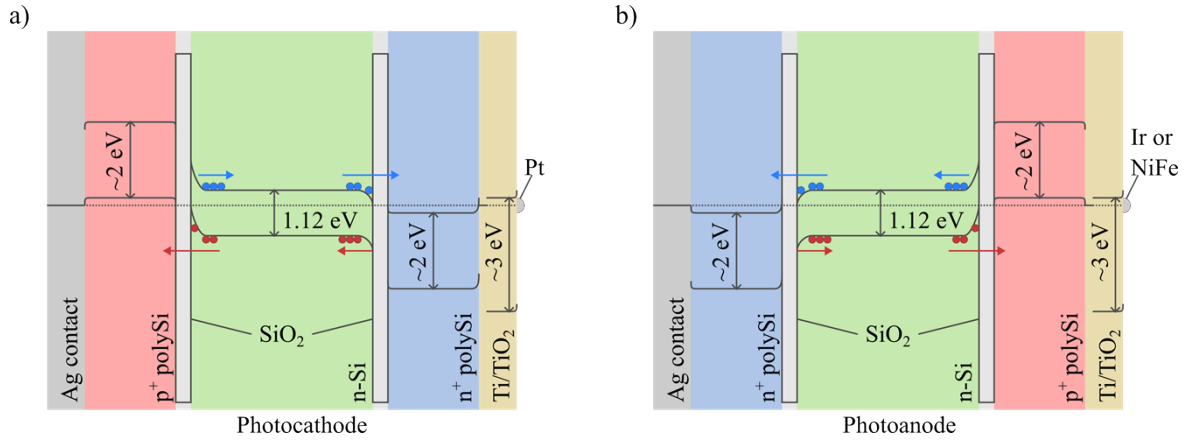

Figure S2 The band diagram of a) photocathode and b) photoanode based on TOPCon Si in dark.

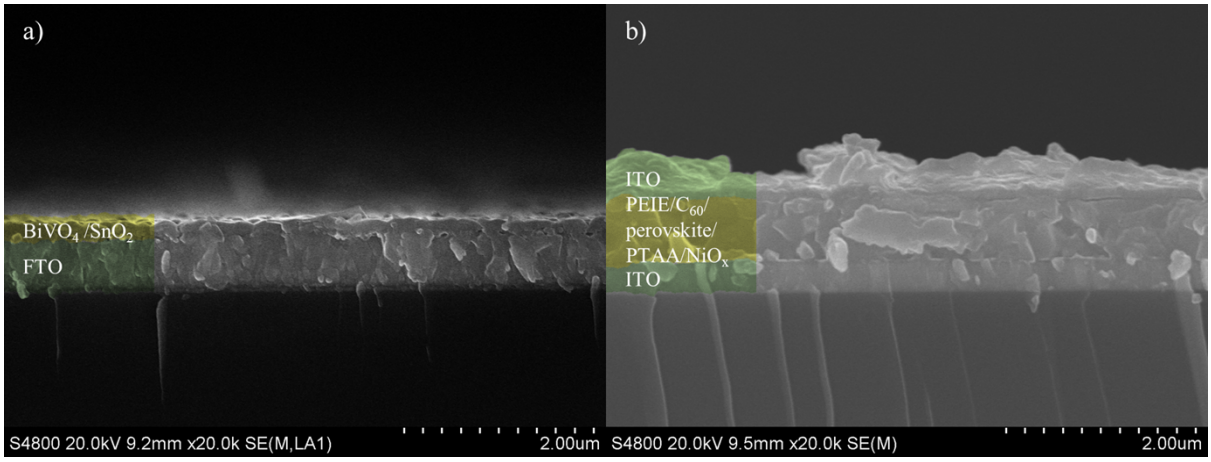

Figure S3 SEM images on a) BiVO4 photoanode and b) halide perovskite photocathode. The SEM image on halide perovskite is taken before transferring the TiO_2 protection over the halide perovskite cell.

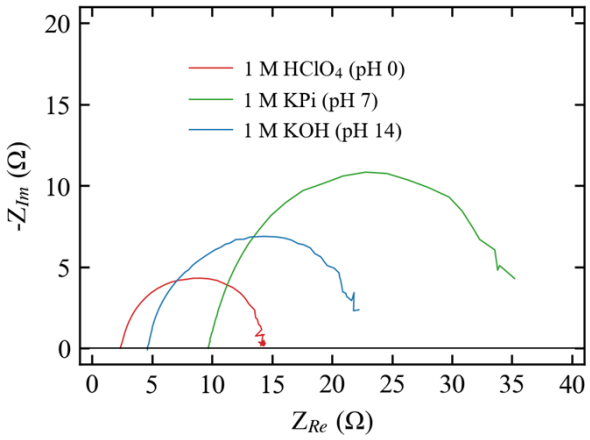

Figure S4 Electrochemical impedance spectroscopy measurements on TOPCon Si photocathodes in various electrolytes over the frequency range of 100 kHz~1 Hz, at 550 mV vs RHE.

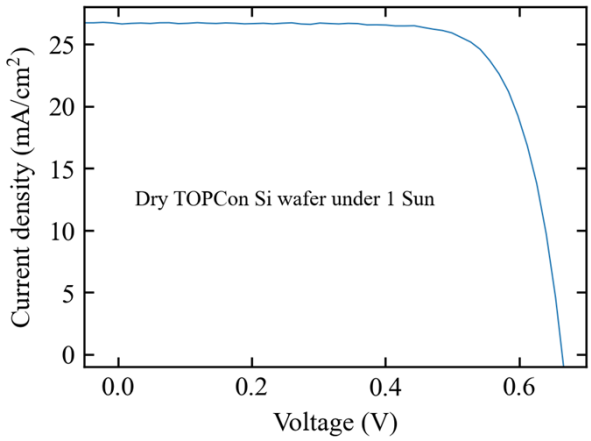

Figure S5 J-V measurement from a dry TOPCon Si wafer showing 664 mV of photovoltage.

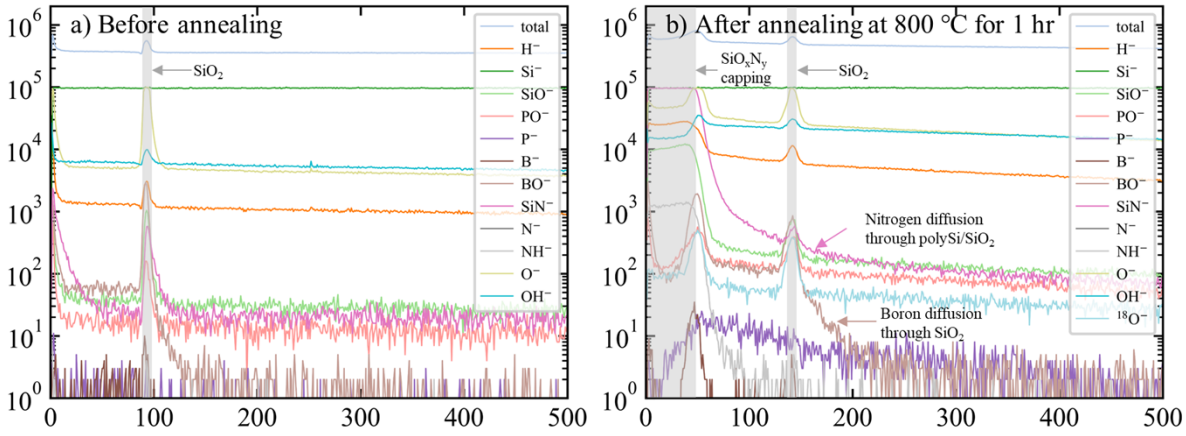

Figure S6 Time-of-flight secondary ion mass spectroscopy (TOF-SIMS) measurement on TOPCon Si a) before and b) after annealing at 800 ℃ for 1 hour. SiN:H capping layers were removed by hydrofluoric acid (2.5 %) before TOF-SIMS measurements, however, the annealed TOPCon Si sample still has the capping layer because the oxidized capping layer

exhibits a slower etch rate.

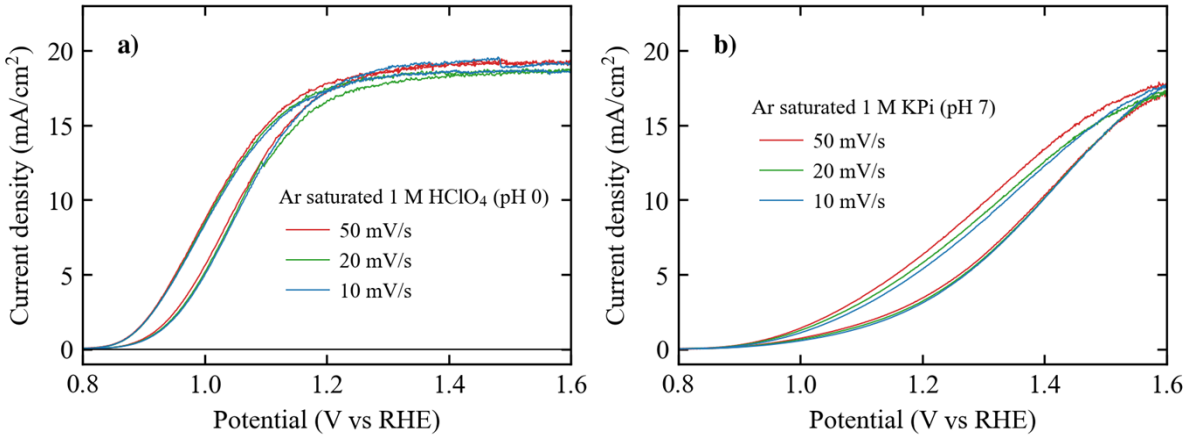

Figure S7 Cyclic voltammetry from a photoanode with Ir catalyst in a) 1 M $HClO_4$ and b) 1 M KPi were measured with various scan rates. The potential gap between the anodic and cathodic scans is 36 mV (at 5 mA/cm^2) in 1 M $HClO_4$ and is not affected by the scan rate. On the other hand, the gap decreases from 104 mV to 84 mV in 1 M KPi.

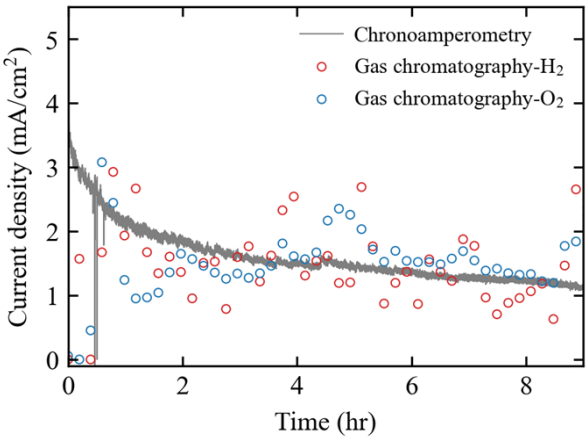

Figure S8 During chronoamperometry of halide perovskite-TOPCon Si photoanode shown in the inset of Figure 6d, H_2 and O_2 products were quantified by gas chromatography (GC) equipped with a thermal conductivity detector and Ar carrier gas. H_2 and O_2 signals were calibrated by using internal standards generating the gases by HER and OER (Pt/Ti or Ir/Ti coated silicon substrates for HER and OER, respectively). Before starting the experiment, the electrochemical cell is saturated with Ar carrier gas to remove H_2 and O_2 background. The flow rate of the carrier gas was 10 sccm (5 sccm for each compartment). The blue and red data points show GC signals in the unit of equivalent current density for easier comparison with the gas chronoamperometry measurement. At the initial moment of the experiment (~ 0.5 hr), there was a time lag between the GC and gas chronoamperometry measurement because it takes time for analytes to diffuse to GC, and it results in a low GC signal at the beginning of the experiment. When calculating Faradaic efficiency, we use a time range between 2 ~ 9 hr to avoid the measurement artifact at the beginning of the experiment. The Faraday efficiency toward HER and OER are 108 and 98 %, respectively. We also consider that the intermittent deviation of the GC signal from chronoamperometry by ~1 mA/cm^2 scale could be related to the bubble stacking and removal on the reaction area.

Silicon Photocathodes					
Year	First author	Electrolyte pH	Photovoltage (mV)	Charge separation	Contact on c-Si

This work	**Moon**	**0**	**645±11**	**MIS**	**Pt/Ti/polySi/SiO_2**
2013	Seger[1]	0	520	p-n	Pt/TiO_2/Ti
2015	Ji[2]	0	450	SLJ	Pt/Ti/$SrTiO_3$
2017	Bae[3]	0	584	MIS	Pt/TiO_2/Ti/polySi/SiO_2
This work	**Moon**	**7**	**636±8**	**MIS**	**Pt/Ti/polySi/SiO_2**
This work	**Moon**	**14**	**641±1**	**MIS**	**Pt/Ti/polySi/SiO_2**
2019	Cui[4]	14	500	p-n	Pt/TiO_2
2020	Liu[5]	0	620	SHJ	Pt/TiO_2/a-Si
Silicon Photoanodes					
Year	First author	Electrolyte pH	Photovoltage (mV)	Charge separation	Contact on c-Si
This work	**Moon**	**0**	**651±11**	**MIS**	**Ir/Ti/polySi/SiO_2**
2015	Mei[6]	0	500	p-n	IrO_2/Ir/TiO_2/Ti
2016	Scheuermann[7]	0	620	MIS	Ir/SiO_2
2016	Scheuermann[8]	0	630	p-n	Ir/TiO_2/SiO_2
This work	**Moon**	**7**	**647±19**	**MIS**	**Ir/Ti/polySi/SiO_2**
This work	**Moon**	**14**	**649±5.5**	**MIS**	**$Ni_{0.8}Fe_{0.2}$/Ti/polySi/SiO_2**
2014	Hu[9]	14	520	p-n	Ni/TiO_2
2015	Sun[10]	14	510	p-n	NiO_x
2017	Yu[11]	14	490	SLJ	$Co(OH)_2$/TiO_2
2018	Moreno-Hernandez[12]	14	620	MIS	Ni/SnO_x/SiO_x
2018	Digdaya[13]	14	538	MIS	Ni/Pt/Al_2O_3/SiO_x
2015	Wang[14]	14	637	SHJ	Ni/ITO/p:a-Si:H/i:a-Si:H
2020	Hemmerling[15]	14	480	MIS	Ir/HfO_2
2020	Chuang[16]	14	570	MIS	Ni/TiO_2

Table S1 Table of photovoltages measured from Si photoelectrodes.

Tandem PEC devices with crystalline silicon bottom cell					
Year	First author	Top cell (band gap, eV)	Bottom cell (band gap, eV)	STH (%)	Lifetime-H_2 (ml cm^{-2})
This work	**Moon**	**$BiVO_4$ (2.4)**	**Si (1.12)**	**0.24**	**1.5**
This work	**Moon**	**Halide perovskite (1.68)**	**Si (1.12)**	**3.6**	**6**
2013	Liu[17]	TiO_2 NW (3.2)	Si nanowire (1.12)	0.12	0.44
2016	Xu[18]	$BiVO_4$ (2.4)	Si nanowire (1.12)	0.2	0.18
2017	Chakthranont[19]	$BiVO_4$ (2.4)	Si nanowire (1.12)	0.45	0.13
2019	Vijselaar[20]	Cu_2O (2.0)	Si nanowire (1.12)	0	N/A
Tandem PEC devices based on earth-abundant materials					
Year	First author	Top cell (band gap)	Bottom cell (band gap)	STH (%)	Lifetime-H_2 (ml cm^{-2})
1988	Sakai[21]	a-Si (N/A)	a-Si (N/A)	1.98	N/A

2006	Ingler[22]	Fe_2O_3 (2.0)	Fe_2O_3 (2.0)	0.11	N/A
2014	Bornoz[23]	$BiVO_4$ (2.4)	Cu_2O (2.0)	0.5	0.053
2018	Shao[24]	TiO_2 (3.2)	P_3HT:PCBM (1.9)	0.16	0.22
2018	Pan[25]	$BiVO_4$ (2.4)	Cu_2O (2.0)	3	12.5
2020	Yang[26]	$BiVO_4$ (2.4)	Sb_2S_3 (1.2)	1.5	4.2
2021	Zhang[27]	$BiVO_4$ (2.4)	Cu_2O (2.0)	3.2	2.2
2021	Huang[28]	$BiVO_4$ (2.4)	CZTS (1.5)	3.17	20.9
2021	Ye[29]	$BiVO_4$ (2.4)	PBDB-T:ITIC:PC_{71}BM (1.7)	4.3	1.3

Table S2. Table of STH efficiency and lifetime H_2 measured from PEC devices based on two or three photoabsorbers. Lifetime-H_2 represents the total amount of hydrogen produced over the lifetime of a PEC device. The lifetime-H_2 refers to a stability test with gas collection (e.g. gas chromatography) when it is available or was estimated from the amount of electrical charge passed during a chronoamperometry.

References

1 B. Seger, D. S. Tilley, T. Pedersen, P. C. K. Vesborg, O. Hansen, M. Grätzel and I. Chorkendorff, *RSC Adv.*, 2013, **3**, 25902.

2 L. Ji, M. D. McDaniel, S. Wang, A. B. Posadas, X. Li, H. Huang, J. C. Lee, A. A. Demkov, A. J. Bard, J. G. Ekerdt and E. T. Yu, *Nat. Nanotechnol.*, 2015, **10**, 84–90.

3 D. Bae, T. Pedersen, B. Seger, B. Iandolo, O. Hansen, P. C. K. Vesborg and I. Chorkendorff, *Catal. Today*, 2017, **290**, 59–64.

4 W. Cui, T. Moehl, S. Siol and S. D. Tilley, *Sustain. Energy Fuels*, 2019, **3**, 3085–3092.

5 B. Liu, S. Feng, L. Yang, C. Li, Z. Luo, T. Wang and J. Gong, *Energy Environ. Sci.*, 2020, **13**, 221–228.

6 B. Mei, T. Pedersen, P. Malacrida, D. Bae, R. Frydendal, O. Hansen, P. C. K. Vesborg, B. Seger and I. Chorkendorff, *J. Phys. Chem. C*, 2015, **119**, 15019–15027.

7 A. G. Scheuermann, J. P. Lawrence, K. W. Kemp, T. Ito, A. Walsh, C. E. D. Chidsey, P. K. Hurley and P. C. McIntyre, *Nat. Mater.*, 2016, **15**, 99–105.

8 A. G. Scheuermann, J. P. Lawrence, A. C. Meng, K. Tang, O. L. Hendricks, C. E. D. Chidsey and P. C. McIntyre, *ACS Appl. Mater. Interfaces*, 2016, **8**, 14596–14603.

9 S. Hu, M. R. Shaner, J. A. Beardslee, M. Lichterman, B. S. Brunschwig and N. S. Lewis, *Science (80-.).*, 2014, **344**, 1005–1009.

10 K. Sun, M. T. McDowell, A. C. Nielander, S. Hu, M. R. Shaner, F. Yang, B. S. Brunschwig and N. S. Lewis, *J. Phys. Chem. Lett.*, 2015, **6**, 592–598.

11 Y. Yu, Z. Zhang, X. Yin, A. Kvit, Q. Liao, Z. Kang, X. Yan, Y. Zhang and X. Wang, *Nat. Energy*, 2017, **2**, 17045.

12 I. A. Moreno-Hernandez, B. S. Brunschwig and N. S. Lewis, *Adv. Energy Mater.*, 2018, **8**, 1801155.

13 I. A. Digdaya, B. J. Trześniewski, G. W. P. Adhyaksa, E. C. Garnett and W. A. Smith, *J. Phys. Chem. C*, 2018, **122**, 5462–5471.

14 H.-P. Wang, K. Sun, S. Y. Noh, A. Kargar, M.-L. Tsai, M.-Y. Huang, D. Wang and J.-H. He, *Nano Lett.*, 2015, **15**, 2817–2824.

15 J. Hemmerling, J. Quinn and S. Linic, *Adv. Energy Mater.*, 2020, **10**, 1903354.

16 C.-H. Chuang, Y.-Y. Lai, C.-H. Hou and Y.-J. Cheng, *ACS Appl. Energy Mater.*, 2020, **3**, 3902–3908.

17 C. Liu, J. Tang, H. M. Chen, B. Liu and P. Yang, *Nano Lett.*, 2013, **13**, 2989–2992.

18 P. Xu, J. Feng, T. Fang, X. Zhao, Z. Li and Z. Zou, *RSC Adv.*, 2016, **6**, 9905–9910.

19 P. Chakthranont, T. R. Hellstern, J. M. McEnaney and T. F. Jaramillo, *Adv. Energy Mater.*, 2017, **7**, 1701515.

20 W. Vijselaar, P. P. Kunturu, T. Moehl, S. D. Tilley and J. Huskens, *ACS Energy Lett.*, 2019, **4**, 2287–2294.

21 Y. Sakai, S. Sugahara, M. Matsumura, Y. Nakato and H. Tsubomura, *Can. J. Chem.*, 1988, **66**, 1853–1856.

22 W. B. Ingler and S. U. M. Khan, *Electrochem. Solid-State Lett.*, 2006, **9**, G144.

23 P. Bornoz, F. F. Abdi, S. D. Tilley, B. Dam, R. van de Krol, M. Graetzel and K. Sivula, *J. Phys. Chem. C*, 2014, **118**, 16959–16966.

24 D. Shao, L. Zheng, D. Feng, J. He, R. Zhang, H. Liu, X. Zhang, Z. Lu, W. Wang, W. Wang, F. Lu, H. Dong, Y. Cheng, H. Liu and R. Zheng, *J. Mater. Chem. A*, 2018, **6**, 4032–4039.

25 L. Pan, J. H. Kim, M. T. Mayer, M.-K. Son, A. Ummadisingu, J. S. Lee, A. Hagfeldt, J. Luo and M. Grätzel, *Nat. Catal.*, 2018, **1**, 412–420.

26 W. Yang, J. H. Kim, O. S. Hutter, L. J. Phillips, J. Tan, J. Park, H. Lee, J. D. Major, J. S. Lee and J. Moon, *Nat. Commun.*, 2020, **11**, 861.

27 Y. Zhang, H. Lv, Z. Zhang, L. Wang, X. Wu and H. Xu, *Adv. Mater.*, 2021, **33**, 2008264.

28 D. Huang, K. Wang, L. Li, K. Feng, N. An, S. Ikeda, Y. Kuang, Y. Ng and F. Jiang, *Energy Environ. Sci.*, 2021, **14**, 1480–1489.

29 S. Ye, W. Shi, Y. Liu, D. Li, H. Yin, H. Chi, Y. Luo, N. Ta, F. Fan, X. Wang and C. Li, *J. Am. Chem. Soc.*, 2021, **143**, 12499–12508.